CONTACT DYNAMICS SIMULATION FOR CAPTURE OPERATION BY SNARE WIRE TYPE OF END EFFECTOR

Satoko Abiko[(1)], Naohiro Uyama[(1)], Tetsuya Ikuta[(1)], Kenji Nagaoka[(1)], Kazuya Yoshida[(1)], Hiroki Nakanishi[(2)], and Mitsushige Oda[(3)]

[(1)] *Tohoku University, 6-6-01, Aramaki-aza Aoba, Sendai, Miyagi, 980-8579, Japan, satoko.abiko@ieee.org, {uyama, ikuta, nagaoka, yoshida}@astro.mech.tohoku.ac.jp*

[(2)]*Japan Aerospace Exploration Agency (JAXA), 2-1-1, Sengen, Tsukuba, Ibaraki, 305-8505, Japan, nakanishi.hiroki@jaxa.jp*

[(3)]*Tokyo Institute of Technology, 2-11-1, Ookayama, Meguro-ku, Tokyo, 152-8550, Japan, oda.m.ab@m.titech.ac.jp*

ABSTRACT

This paper presents contact dynamics simulation for capturing a floating target by long-reach space manipulator systems. Current space manipulator systems have a snare wire type of end-effector. Contact phenomena between the wire and the target have not been completely clarified yet and the behavior of the manipulator and the target after contact is not easy to evaluate. Therefore, contact dynamics model is a key to achieve accurate dynamic simulation in capture operation. In this paper, characteristics of contact dynamics between the wire and a rigid object, especially the stiffness of the wire, are identified through experiment. By using the identified properties, the contact dynamics simulation between JEM Remote Manipulator System (JEMRMS) and a floating target is carried out.

Key words: Contact dynamics; Snare wire; Capture operation; Flexible space manipulator.

1. INTRODUCTION

Autonomous space transportation systems are key technologies to diversify space use in both manned and unmanned operations in the future. The H-II Transfer Vehicle (HTV) is one of the existing space transportation systems and is a cargo liner to the International Space Station (ISS). The HTVs have been successfully docked to the ISS by the technology of capture-berthing system in which the HTV autonomously approaches to the ISS and then, is captured by Space Station Remote Manipulator System (SSRMS) as shown in Fig. 1 [1]. First commercial orbital transportation service system named Dragon also adopts the capture-berthing system and was perfectly docked to the ISS in June 2012 [2]. In such space activities, necessary contact between the space manipulator and the target occurs and accidental contact may happens. Therefore, to evaluate the fidelity of the systems in the operations, contact dynamics is a key to accomplish orbital missions.

Figure 1: Capture of HTV by SSRMS ©JAXA

On the other hand, current space manipulators such as the SSRMS and Shuttle Remote Manipulator System (SRMS) are equipped with an end-effector called Latching End-Effector (LEE). The LEE has three snare wires inside as shown in Fig. 2 and it tightly squeezes a Grapple Fixture (GF) of a target. The space manipulators are generally used to transfer on-board payloads on the ISS, grasp floating targets such as the HTV, and serve as the platform for astronauts in the Extra Vehicular Activity (EVA). Among such tasks, it is demanded to ensure secure grasp in the capture operation. Especially, when the manipulator grasps a floating target, if contingent collision happens, the manipulator and the target may be damaged or the target may move away from the secure capturing area. Therefore, a precise dynamic simulation including the contact phenomena is required for safe capture in such orbital missions. However, the contact phenomena between the flexible snare wire and the rigid object are rather complicated and have not been completely clarified yet.

In this paper, we develop contact dynamics simulator for

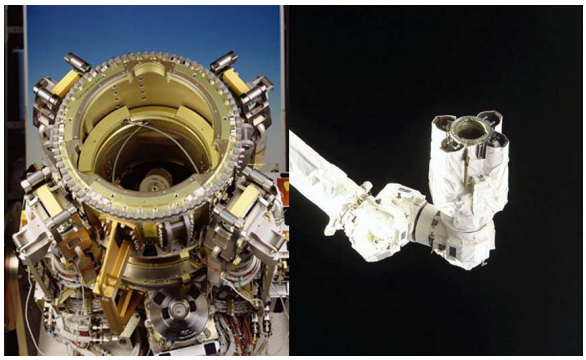

Figure 2: Latching End Effector of SSRMS ©MDA

capture operation by the snare wire type of end effector. The developed simulator can be useful to predict the dynamic motion of the target and the manipulator after contact in real-time and evaluate their motion if contingent contact occurs. However, the snare wires are generally fixed both ends without tension and have geometric configuration at the beginning as shown in Fig. 2. This condition of the wire is also considered that the wire is buckling due to very small compression forces at both ends. In the above condition, it is difficult to analytically model the contact dynamics of the loose wire because the model of the loose wire is expressed with partial differential equation and the shape of it is obtained by complete elliptic integrals in theory. Especially, when the wire has initial shape, the analytical solution becomes more complex. Additionally, with the elliptic integrals, the convergent calculation is required to derive the shape of the wire from the applied force. This calculation requires a lot of computational consuming and it may not converge to real solution and drop into local minima.

This paper examines the characteristics of contact dynamics between the wire and a rigid object, especially the stiffness of the wire through experiment. Through the experiment, the dominant parameters of the contact dynamics are found out which influence the behavior of the space manipulator and the target during and after contact. By using the identified characteristics of the wire, the contact dynamics simulation between the JEMRMS and a target is carried out.

2. OVERVIEW OF CONTACT DYNAMICS SIMULATOR

Figs. 3 and 4 show an overview of contact dynamics simulator and display of the simulator, respectively. The simulator consists of mainly four parts, namely:

(1) dynamics model of flexible space manipulator

(2) dynamics model of an orbital payload

(3) contact dynamics model

(4) real time collision detection

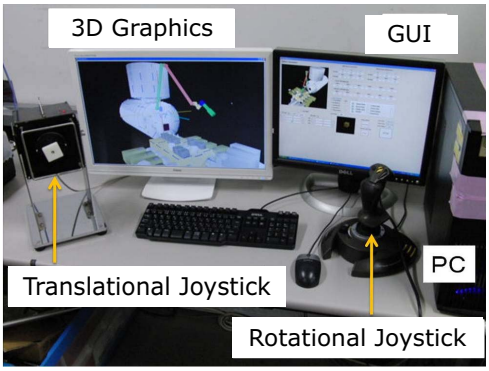

Figure 3: Overview of the simulator

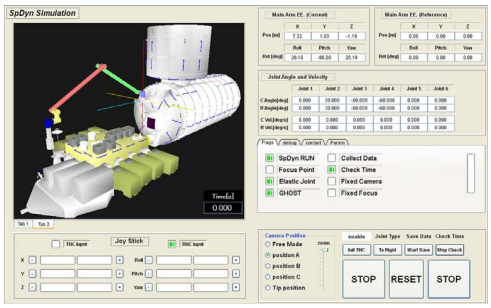

Figure 4: Display of the simulator

The dynamic models of the space manipulator and the payload are separately developed. When the contact between them is detected by the real time collision detection, the interactive force between them are induced based on the contact dynamics model. The real time collision detection is developed based on [3]. The orbital payload is assumed to be one rigid body in this paper. Then, the important elements are dynamics model of the space manipulator and the contact dynamics model. The detail of them are expressed in the following sections.

3. DYNAMICS OF SPACE MANIPULATOR SYSTEM

The space manipulator systems have generally flexible joints. This kind of manipulator systems are modeled with the stiffness of each joint as follows [4]:

$$\boldsymbol{H}\ddot{\boldsymbol{q}} + \boldsymbol{c}(\boldsymbol{q}, \dot{\boldsymbol{q}}) + \boldsymbol{K}\left(\boldsymbol{q} - \boldsymbol{q}_m\right) = \boldsymbol{J}^T \mathcal{F}_e \qquad (1)$$

$$\boldsymbol{B}\ddot{\boldsymbol{q}}_m + \boldsymbol{D}\dot{\boldsymbol{q}}_m - \boldsymbol{K}\left(\boldsymbol{q} - \boldsymbol{q}_m\right) = \boldsymbol{\tau} \qquad (2)$$

where each symbol is listed in Tab. 1. In the table, n denotes the degrees-of-freedom (DOF) of the manipulator.

3.1. Nonlinear characteristics of flexible joint

It was observed that the JEMRMS has nonlinear characteristics on each flexible joint in the ground experiment before the launch [5]. The Japanese space agency (JAXA) then conducted orbital experiment to measure the joint characteristics by the step-response of first joint in

Table 1: notations in eqs. (1) and (2)

$\boldsymbol{q}$	$\in R^{n\times 1}$	:	angle of output axis.
$\boldsymbol{q}_m$	$\in R^{n\times 1}$	:	angle of motor axis.
$\boldsymbol{H}$	$\in R^{n\times n}$	:	inertia matrix of the manipulator.
$\boldsymbol{B}$	$\in R^{n\times n}$	:	inertia matrix of the motor.
$\boldsymbol{c}(\boldsymbol{q}, \dot{\boldsymbol{q}})$	$\in R^{n\times 1}$	:	coriolis, centripetal and gravitational forces and torques.
$\boldsymbol{D}$	$\in R^{n\times 1}$	:	viscous damping coefficient of the motor.
$\mathcal{F}_e$	$\in R^{6\times 1}$	:	force and moment exerted on the end-effector.
$\boldsymbol{J}$	$\in R^{6\times n}$	:	Jacobian matrix with respect to the end-effector.
$\boldsymbol{\tau}$	$\in R^{n\times 1}$	:	torque on the joints.
$\boldsymbol{K}$	$\in R^{n\times n}$	:	stiffness of the joints.

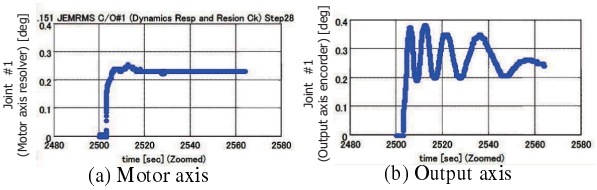

(a) Motor axis (b) Output axis

Figure 5: Orbital experiment ©JAXA

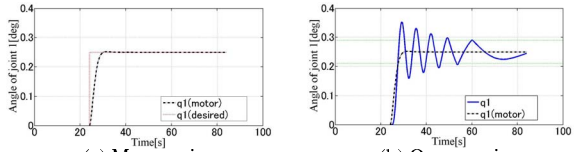

(a) Motor axis (b) Output axis

Figure 6: Simulation result

orbit. Fig. 5 shows an example result of orbital experiment published in Japanese domestic conference. As seen in the figure, the joint has the nonlinearity and the frequency of oscillation varies. In this paper, we estimated the observed characteristics and applied it to the dynamics model of the JEMRMS. Through the identification, we determined the stiffness and viscous characteristics of joints as listed in Tab. 2. Fig. 6 shows the numerical simulation with the estimated joint characteristics. As seen in the figure, we could reproduce almost same characteristics with the determined parameters. In the estimation, we focused on the high frequency on the

Table 2: Determined characteristics of joints

$\Delta\boldsymbol{q} = \boldsymbol{q} - \boldsymbol{q}_m$ [deg]	Stiffness $\boldsymbol{K}_n$ [Nm/deg]	Viscosity $\boldsymbol{D}_n$ [Nms/deg]
$\lvert\Delta\boldsymbol{q}\rvert < 0.04$	12.5	48.9
$0.04 \leq \lvert\Delta\boldsymbol{q}\rvert < 0.06$	475	87.3
$0.06 \leq \lvert\Delta\boldsymbol{q}\rvert$	475	17.6

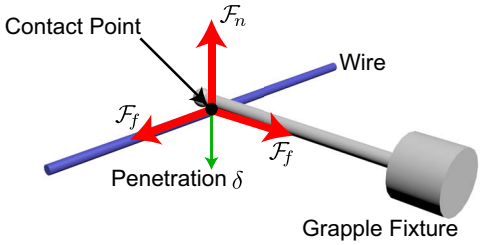

Figure 7: Contact model of wire

first two vibrations since the period right after the contact is important in the contact dynamics simulation. For more precise fitting, we need to improve the parameter settings.

4. CONTACT DYNAMICS OF SNARE WIRE

This section describes the contact dynamics model with the wire and the stiff GF. Fig. 7 shows an overview of the contact model. The contact force can be expressed with the normal force and the frictional force.

The normal force $\mathcal{F}_n$ in contact dynamics of the rigid bodies is generally modeled as the following nonlinear model with penetration δ, stiffness k, and viscous damping c.

$$\mathcal{F}_n = k\delta^p + cG(\delta)\dot{\delta}^q \tag{3}$$

where $G(\delta)$ denotes the function regarding to the penetration δ, p, and q represent arbitrary constants[6].

When we determine $G(\delta) = 1, p = 1, q = 1$, eq. (3) becomes the linear spring-dashpot model as follows:

$$\mathcal{F}_n = k\delta + c\dot{\delta} \tag{4}$$

In this case, the problem amounts to the determination of the constants k and c in eq. (4).

As for the frictional force, $\mathcal{F}_f$, with which the slip on the surface of the object occurs, the Coulomb friction model is applied in this paper.

$$\mathcal{F}_f = \mu\mathcal{F}_n \tag{5}$$

where μ represents coefficient of kinetic friction.

In the contact between the wire and the GF, the deflection of the wire due to the external force is considered the penetration in the contact model. The stiffness can be determined by the relationship between the external force and the penetration through the static experiment. The damping coefficient c is also observed through the dynamic experiment.

4.1. Definition of stiffness of loose wire

The contact model of tensioned wire has been proposed in [7]. In [7], the linear spring-dashpot model was selected as the contact dynamics model and the stiffness is

Table 3: Conditions of the wire

Material	Diameter D [mm]	Length L [mm]	Fixed length l [mm]	Contact position s [mm]
SUS-304	1.5	180	175	40, 65, 90

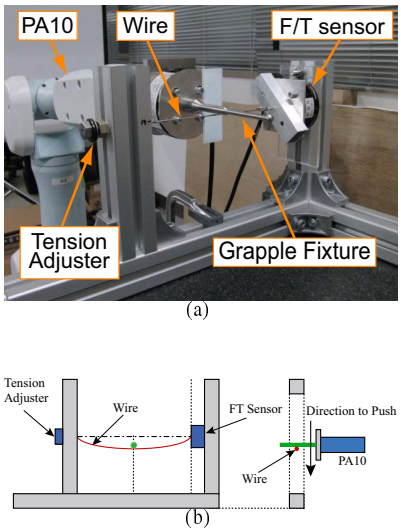

Figure 8: Experimental setup

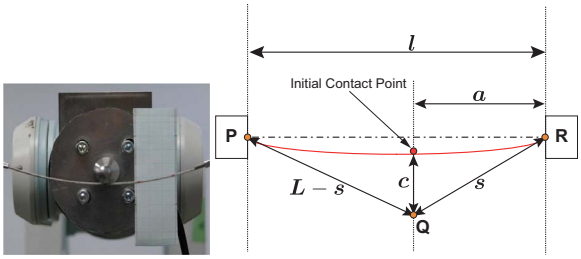

Figure 9: Definition of loose wire

defined as the ratio between the applied force and the deflection. In the tensioned wire model, the exact solution of the stiffness is expressed with flexural rigidity, tension, and contact position. Even in the tensioned wire, the derived stiffness is too complicated. In the real snare wire, it becomes more complex since the snare wire has initially no tension and forms certain geometry, which requires elliptic integrals and convergence condition to obtain the deflection of the wire from the applied force.

Up to now, there is no discussion of the contact dynamics model between the loose wire and the stiff object. As for first attempt, this paper examines the stiffness characteristics of the loose wire through static experiment. In the experiment, the penetration is determined by the displacement from the initial contact position as shown in Fig. 9. The wire is deformed until the maximum displacement Q which is derived by the geometric configuration with the total length L and the fixed length l since our interest is the characteristics of the loose wire and the phenomena after the point Q in Fig. 9 will change due to the stretch of the total length of the wire.

4.2. Experimental estimation of stiffness of loose wire

To evaluate the stiffness of the loose wire, the following static experiment was carried out. Fig. 8 shows the experimental setup of the stiffness estimation. The wire is loosely fixed with fixed ends. One end of the wire is connected to an Force/Torque (F/T) sensor and the other is attached with a tension adjuster. The tension of the wire can be measured and adjusted in the experiment. The basis of the setup has a mechanism to change the distance between both ends of the wire by sliding one end along the axis of the wire. With this mechanism, the condition of the loose wire can arbitrarily be adjusted. The GF mounted on the tip of the industrial robot, PA-10, is used to statically apply enforced displacement perpendicularly with respect to the axis of the wire as shown in Fig. 8(b). The reaction force due to the material properties and the deflection of the wire can be observed by an F/T sensor attached between the GF and the tip of the PA-10.

The condition of the wire in the experiment is as listed in Tab. 3. The total length L was $180[mm]$ and the distance between two ends of the wire l was $175[mm]$. The enforced displacement was applied at three contact positions. Fig. 10 shows the relation between the enforced displacement of the wire and the reaction force. As shown in Fig. 10, the observed reaction force becomes larger when the displacement is getting larger. This means that the stiffness of the wire becomes stiffer when the displacement is getting larger. The result is approximated with the least square method. The approximated results are expressed with the quadratic function $\mathcal{F}_n = A\delta^2 + B\delta + C$ with good correlation R^2 as listed in Tab. 4. In practice, when the penetration $\delta = 0$, the reaction force $\mathcal{F}$ should be zero. However, the observed approximated function had an offset when the penetration $\delta = 0$. This is because the observed data includes measurement error in the experiment. Especially, in the cases of $s = 40[mm]$ and $65[mm]$, the slip of the ends of the wire negatively affects the measurement of the reaction force. To obtain more precise model, further identification experiment should be required. However, we could qualitatively observe the tendency of the wire stiffness that the stiffness becomes larger as the penetration becomes larger. Fig. 11 shows the tendency of the wire stiffness on the assumption that the contact dynamics model is the linear spring-dashpot model.

4.3. Dynamic contact with free-floating target

To compare the numerical simulation with the above stiffness model, we carried out the dynamic contact experiment between the loose wire and a floating target. Fig. 12 shows an overview of the experimental setup. In the experiment, an air-floating target on a horizontal smooth surface table is used to emulate micro-gravity environ-

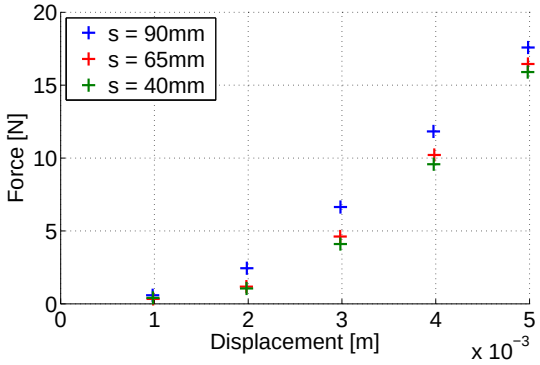

Figure 10: Relation between force and displacement (s=90, 65, 40mm)

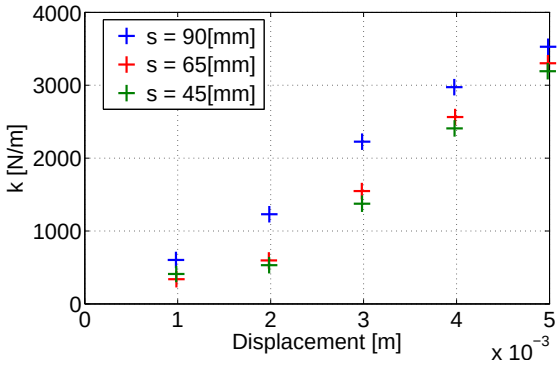

Figure 11: Stiffness in the linear spring-dashpot model

Table 4: Results of wire stiffness identification

s	A	B	C	R^2
40 [mm]	719880	-13.578	0.0533	0.9976
65 [mm]	878089	-1086	0.2115	0.998
90 [mm]	890183	-1297.6	0.3457	0.9975

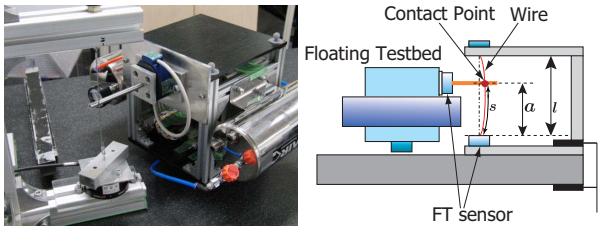

Figure 12: Contact experiment setup

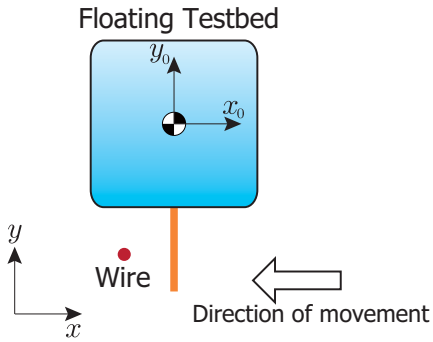

Figure 13: Simulation model of contact experiment

ment. The wire is fixed perpendicularly with respect to the inertial frame on the table. The target is equipped with an F/T sensor on the tip of a probe as shown in the figure. The target moves toward the wire with certain initial velocity. The dynamic motion of the target is observed by a motion capture system. The numerical simulation with the identified contact dynamics model in the previous subsection is carried out to compare the experimental result and to verify the efficiency of the identified contact model listed in Tab. 4.

The wire used in the experiment and dynamic properties of the target are listed in Tab. 5. The contact position s is set to be $90[mm]$ from the bottom end.

Figs. 14, 15, and 16 show the results of the experiment and the numerical simulation. Fig. 14 shows the translation velocity of the center of the mass (CoM) of the target. Fig. 15 shows the angular velocity of the target. Fig. 16 shows the reaction force.

It is observed from the figures that the motion of the target after the contact starts rotating and the translational velocity of the CoM of the target slows down. The target oscillates for a while during the contact and consequently converges to certain velocity. The observed vibrations seemed to be generated during contact with the wire in the experiment. To compare the experimental results with the numerical simulation, the simulation with the identified contact model could reproduce the motion of the target in the experiment. Although the peek of the reaction force has a difference between them, the total impulse during the contact is almost same in the experiment and in the simulation. Therefore, it can be concluded that the developed contact dynamics simulator has enough precision to evaluate the motion of the target before and after the contact.

5. CONTACT DYNAMICS SIMULATION OF JEMRMS

This section presents a contact dynamics simulator for capture operation by a space manipulator system. In this simulator, the floating target captured by the JEMRMS is selected as an application. Fig. 17 shows an overview of the simulation model. The dynamic model of the JEMRMS is designed based on eqs. (1) and (2), and joint char-

Table 5: Condition of the contact dynamics experiment

	D [mm]	L [mm]	l [mm]	s [mm]
wire	1.5	180	175	90

	mass	inertia
target	8.9 [kg]	0.16 [kgm^2]

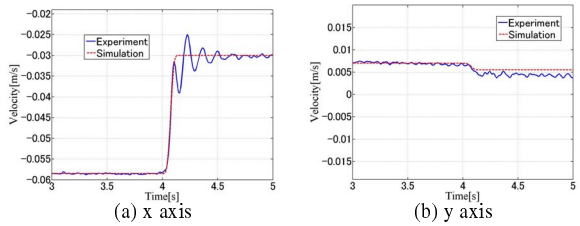

(a) x axis (b) y axis

Figure 14: Velocity

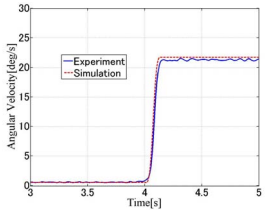

Figure 15: Angular velocity

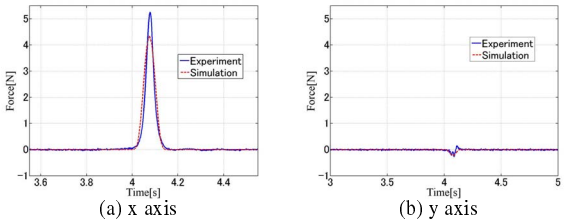

(a) x axis (b) y axis

Figure 16: Force

Table 6: Dynamic properties of the payload

mass [kg]	inertia [kgm^2]		
m	I_{xx}	I_{yy}	I_{zz}
500	415	83	415

acteristics as listed in Tab. 2. The condition of the wire inside the LEE is assumed to be same as listed in Tab. 5. In this simulation, for first attempt, one wire is fixed inside the LEE as shown in Fig. 17. The payload is assumed to move toward the wire in the LEE at $10[m/s]$ along y axis.

Figs. 18 and 19 show the snapshots of the simulation results. Fig. 18 shows the motion of the JEMRMS and the payload in contact and Fig. 19 shows the view from the side of the payload in contact. Figs. 20 and 21 show the joint angles of the JEMRMS, and the observed reaction

Table 7: Dynamic properties of the payload

mass [kg]	inertia [kgm^2]		
m	I_{xx}	I_{yy}	I_{zz}
500	415	83	415

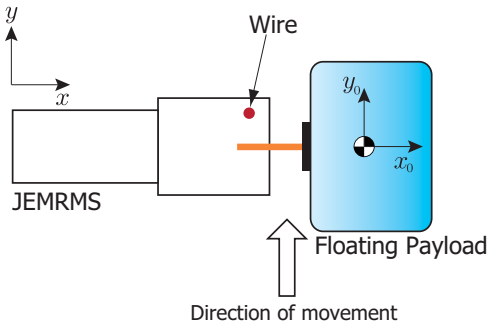

Figure 17: Overview of capture operation by the JEMRMS

force and attitude of the payload, respectively.

As observed in Figs.18 and 19, it is demonstrated that the payload bounces away from the capturing area due to the contact with the snare wire. Fig. 20 shows that the JEMRMS vibrates after the contact with the payload, which makes recovery operation more difficult. Besides, the simulator demonstrates that the payload rotates after the contact, which indicates that the grasping point of the payload escapes away and the payload might cause damage to the ISS.

In the real operation in orbit, the material properties of the wire inside the LEE is different. Therefore, the behavior of the payload after the contact should be different. However, this paper presents the framework of the contact dynamics simulator which is very useful to predict the motion of the target in contact and estimate the emergency cases in simulation. If we could have the knowledge of the material properties of the real wire of the LEE, we are able to demonstrate the capture operation in arbitrary conditions including contingent contact or necessary contact. By using the simulator, it would be possible to provide avoidance of the contact danger with new strategy.

6. CONCLUSION

This paper presented contact dynamic simulator for capture operation by space manipulator system. Current space manipulator system has a mechanism with three snare wires to grasp a target on the end-effector. However, the contact dynamics property with the snare wire is not completely clarified up to now. In this paper, the characteristics of loose wire was examined with static load experiment from the aspect of the contact dynamics. The observed characteristics had tendency that the larger penetration provides larger stiffness. The identified contact dynamics characteristics is applied to a numerical simulator which demonstrates capture operation of a floating target by a flexible space manipulator.

REFERENCES

[1] http://www.jaxa.jp/projects/

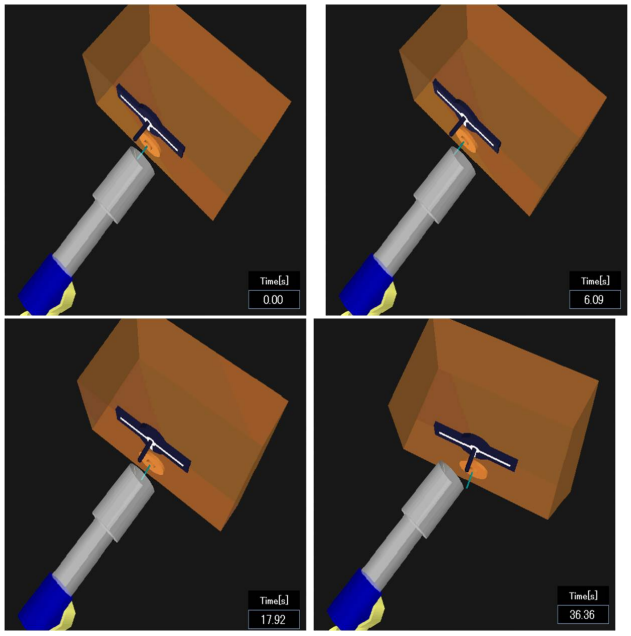

Figure 18: Motion of the JEMRMS and the payload in contact

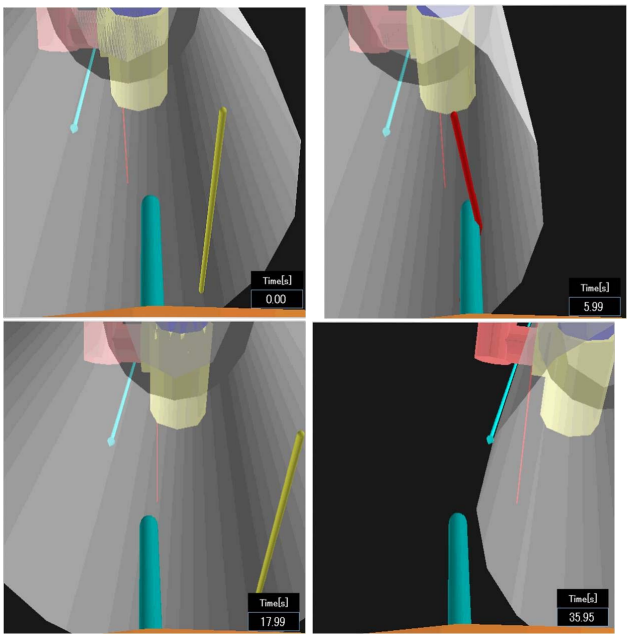

Figure 19: View from the payload in contact

rockets/htv/index_e.html

[2] http://www.spacex.com/dragon.php/

[3] Ericson C., (2004), *Real-Time Collision Detection*, CRC Press.

[4] Spong M. W., (1987), Modeling and Control of Elastic Joint Robots, *Trans. of the ASME,* **109**, 310–319.

[5] Doi S., Wakabayashi Y. Matsuda T.and Satoh N., (2002), JEM Remote Manipulator System, *Journal of the Aeronautical and Space Sciences Japan,* **50**, 7–14.

[6] Gilardi G. and Sharf I., (2002), Literature survey of contact dynamics modelling, *Mechanism and Machine Theory,* **37**, 1213–1239.

[7] Uyama N., Yoshida K., Nakanishi H., Oda M., Sawada H., and Suzuki S., (2011), Contact Dynamics Modeling for Snare Wire Type of End Effector in Capture Operation, *Proc. of the 28th International Symposium on Space Technology and Science*, d-35.

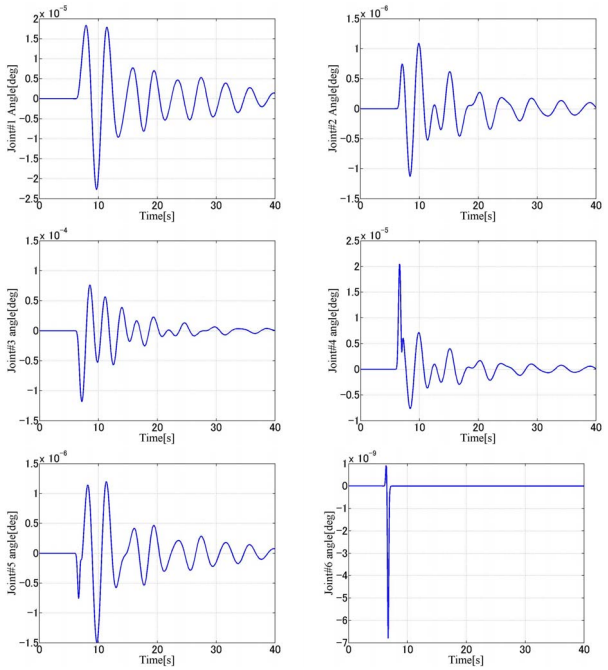

Figure 20: Joint angles of JEMRMS

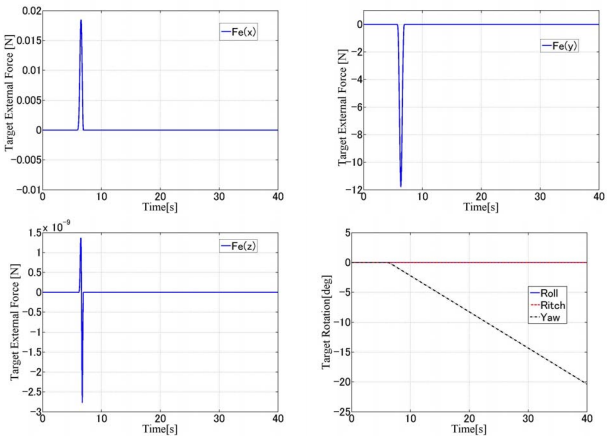

Figure 21: Force and attitude of the payload